Indian Journal of Pure & Applied Physics
Vol. 56, November 2018, pp. 902-913

Use of vibrational spectroscopy to study 1,3-dimethyl-5-nitrobenzene: A combined theoretical and experimental approach

S Seshadri[a]* & M Padmavathy[b]

[a]PG & Research Department of Physics, Urumu Dhanalakshmi College, Kattur, Trichy 620 019, India
[b]Department of Physics, Shrimati Indira Gandhi College, Trichy 620 002, India

Received 18 June 2017; accepted 3 November 2017

The FTIR and FT-Raman spectra of 1,3-dimethyl-5-nitrobenzene (DMNB) have been recorded in the range 4000–400 cm^{-1} and 3500–100 cm^{-1}, respectively. The molecular structures, fundamental vibrational frequencies and intensity of the vibrational bands have been investigated and interpreted theoretically with the use of structural optimizations and normal coordinate force field calculations based on density functional theory (DFT) with 6-31G(d,p) basis set. The vibrational assignments have been made from potential energy distribution (PED). The theoretically simulated vibrational spectra of the molecule show excellent agreement with the experimental spectra. The hyper conjugative interaction energy ($E^{(2)}$) and electron densities of donor (*i*) and acceptor (*j*) bonds have been calculated using NBO analysis. The electronic transition has been studied using UV-Visible analysis of the title molecule with B3LYP/6-31G(d,p) level of theory. The microscopic non-linear optical (NLO) behaviour of the title compound has also been calculated. In addition, the ^{1}H and ^{13}C NMR chemical shifts values of DMNB in the ground state for B3LYP/6-31G(d,p) method have also been calculated using gauge independent atomic orbital (GIAO) method.

Keywords: FTIR, FT-Raman, DFT, UV-Visible, NMR

1 Introduction

Benzene is a colorless and highly flammable liquid with a sweet smell. It is an important industrial solvent and precursor to basic industrial chemicals including drugs, plastics, synthetic rubber and dyes. It evaporates into the air very quickly and dissolves slightly in water[1]. Benzene was historically used as a significant component in many consumer products such as liquid wrench, several paint strippers, rubber cements, spot removers and other hydrocarbon containing products. Benzene is also a natural part of crude oil, gasoline and cigarette smoke[2,3]. Today, benzene is used mainly as an intermediate to make other chemicals. Its most widely produced derivatives include styrene, which is used to make polymers and plastics, phenol for resins and adhesives and cyclohexane which is used in the manufacture of nylon.

Nitrobenzene is used to produce lubricating oils used in motors and machinery. Nitrobenzene and its derivatives are used in the manufacture of dyes, drugs, pesticides, polisher, paint and synthetic rubber. Nitrobenzene is also used to mask unpleasant odors in shoe and floor polishes, leather dressings, paint solvents and other materials. A significant use of nitrobenzene is its use in the production of the analgesic paracetamol and it has been used as an inexpensive perfume for soaps. Dimethylbenzene is used as an additive to motor oils, as a crystallizing solvent, and in the production of the synthetic intermediate phenyl magnesium bromide. Dimethylbenzene is used in the fumigant and insecticide, solvent and chemical intermediate to manufacture dyes, agrochemicals, pharmaceuticals and other organic synthesis.

Various spectroscopic studies of halogen and nitrogen substituted benzene compounds have been reported in the literature[4-8]. DMNB belongs to the group of organic halogen compounds replacing two hydrogen atoms in benzene by methyl (CH_3) and a nitro group (NO_2). Literature survey reveals that no detailed B3LYP with 6-31G(d,p) basis set calculations, NBO and NLO analysis, UV-Visible studies and NMR chemical shifts calculation of DMNB have been reported so far. It is, therefore thought worth to make this theoretical and experimental vibrational spectroscopic research based on molecular structure to give the correct assignment of fundamental bands in the experimentally observed FTIR and FT-Raman spectra. In this study, molecular geometry, optimized parameters and vibrational frequencies are computed

*Corresponding author
(E-mail:ssudc@14gmail.com)

using hybrid density functional method. These methods predict relatively accurate molecular structure and vibrational spectra with moderate computational effort.

2 Experimental Details

The fine sample of 1,3-dimethyl-nitrobenzene (DMNB) was purchased from Sigma-Aldrich chemicals, USA and it was used as such without any further purification. The FTIR spectrum of the compound has been recorded in Perkin-Elimer 180 spectrometer in the range of 4000–400 cm^{-1}. The spectral resolution is ±2 cm^{-1}. The FT-Raman spectrum of the compound was also recorded in same instrument with FRA 106 Raman module equipped with Nd: YAG laser source operating in the region 3500–100 cm^{-1}at 1064 nm line width with 200 Mw powers. The UV absorption spectrum is registered in ethanol on Shimadzu UV-1800 PC spectrophotometer in the spectral region 800–100 nm.^{13}C and ^{1}H NMR spectra were taken in CDCl3 solutions and all signals were referenced to TMS on a BRUKER TPX-400 FT-NMR spectrometer.

3 Computational Details

The molecular structure of the title compound in the ground state is computed by B3LYP/6-31G(d,p) method. The optimized structural parameters are used in the vibrational frequency calculations at B3LYP level. The DFT calculations were carried out for DMNB with GAUSSIAN 09W program package[9]. Initial geometry generated from the standard geometrical parameters was minimized without any constraint, which invokes Becke's three parameter hybrid method[10] using the correlation function of Lee *et al.*[11], implemented with the same basis set for better description of the bonding properties. All the parameters were allowed to relax and all the calculations converged to an optimized geometry which corresponds to a true minimum, as revealed by the lack of imaginary values in the wave number calculations. The cartesian representation of the theoretical force constants has been computed at the fully optimized geometry.

The multiple scaling of the force constants was performed according to scaled quantum mechanical (SQM) procedure[12] using linear scaling in the natural internal coordinate representation[13]. Transformation of force field, the subsequent normal coordinate analysis (NCA) including the least square refinement of the scale factors and calculation of the potential energy distribution (PED) were done on a PC with the MOLVIB program (version V7.0-G77) written by Sundius[14,15]. The calculated frequencies are scaled by 0.9689 scale factor[16,17]. As a result, the unscaled frequencies, reduced masses, force constants, infrared intensities and Raman activities were obtained. The systematic comparison of the results from DFT theory with results of experiments has shown that the method using B3LYP functional is the most promising in providing correct vibrational wave numbers.

The Raman activities (S_i) calculated by the Gaussian 09W program was converted to relative Raman intensities (I_i) using the following relationship derived from the intensity theory of Raman scattering[18,19]:

$$I_i = \frac{f(\nu_0 - \nu_i)^4 S_i}{\nu_i\left[1 - \exp(-hc\nu_i / KT)\right]} \quad \ldots (1)$$

where ν_0 is the laser exciting wavenumber in cm^{-1} (in this work, we have used the excitation wavenumber ν_0 = 9398.5 cm^{-1}, which corresponds to the wavelength of 1064 nm of a Nd:YAG laser), ν_i is the vibrational wavenumber of the i^{th} normal mode (cm^{-1}), while S_i is the Raman scattering activity of the normal mode ν_i, f (is a constant equal to 10^{-12}) is a suitably chosen common normalization factor for all peak intensities h, k, c and T are Planck and Boltzmann constants, speed of light and temperature in Kelvin, respectively.

In this study, the ^{13}C and ^{1}H NMR chemical shifts and nuclear magnetic shielding tensor values of DMNB in the ground state for B3LYP/6-31G(d,p) method were calculated with the gauge independent atomic orbital (GIAO) method[20,21]. The electronic absorption spectra for optimized molecule are also calculated for the same basis set. Further, the NBO analysis and NLO activity of the title compound were calculated using DFT method. All calculations were performed using Gaussian 09W program package[9] employing B3LYP method with 6-31G(d,p) basis set.

4 Results and Discussion

4.1 Molecular geometry

The optimized molecular structure of DMNB along with numbering of atoms is shown in Fig. 1. The optimized geometrical parameters of title molecule obtained by DFT-B3LYP/6-31G(d,p) level are listed in Table 1. From the structural data given in Table 1, it is observed that the various bond lengths are found to be almost same at B3LYP/6-31G(d,p) level of theory. The calculated geometrical parameters were compared with X-ray diffraction result[22,23]. However,

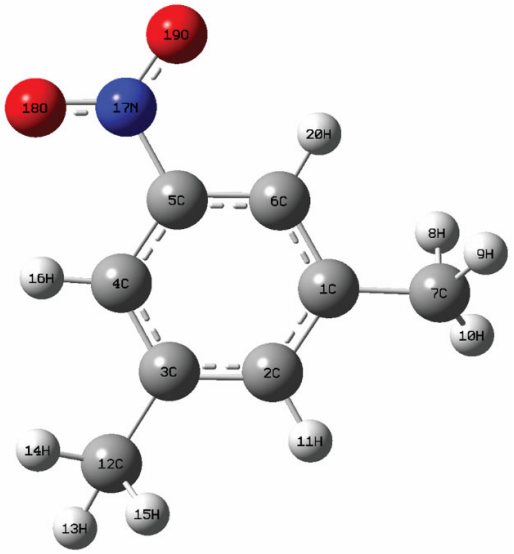

Fig. 1 — Molecular structure of DMNB.

the same level of theory, in general slightly over estimates bond lengths but it yields bond angles in excellent agreement with experimental values. The calculated geometric parameters can be used as foundation to calculate the other parameters for the compound.

The optimized molecular structure of DMNB reveals that the two methyl and a nitro groups are in planar with the heterocyclic ring. Inclusion of CH_3 and NO_2 groups is known for its strong electron-with drawing nature. It is expected to increase a contribution of the resonance structure, in which the electronic charge is concentrated at this site. This is the reason for the longer of bond lengths C2–H11=1.087 Å, C4–H16= 1.083 Å and C6–H20=1.083 Å compared to experimental values of same bond lengths. The methyl C–H bond lengths are greater with aromatic C–H values. The carbon atoms are bonded to the hydrogen atoms with π-bond in heterocyclic ring and the substitution of CH_3 atoms for hydrogen reduces the electron density at the ring carbon atom. The carbon atoms in substituted to heterocyclic ring exert a larger attraction on the valence electron cloud of the hydrogen atom resulting in an increase in the CH_3 force constants and a decrease in the corresponding bond length.

The aromatic C–C bond distances of DMNB are found to have higher values in theoretical calculation than experimental values. Generally, the C–C bonds in aromatic ring are not of the same length. The differences between the C–C bond distances are small. But knowing that electronegative substituent on CH_3 and NO_2 group trend to longer the C–C bonds adjacent to the substituent, we assumed that the bond lengths are slightly decreasing order C1–C7, C3–C12, C1–C2, C2–C3, C1–C6, C3–C4, C4–C5 and C5–C6. Due to the effect and methyl group, the bond lengths C1–C7 and C3–C12 elongates. The CH_3 group substitution bond angles C2–C1–C7, C6–C1–C7, C2–C3–C12 and C4–C3–C12 which are calculated at 120.846º, 120.699º, 120.831º and 120.713º and are smaller than typical aromatic ring angles of 119º and 118º.

4.2 Vibrational assignments

Normal coordinate analyses were carried out for the title compound to provide a complete assignment of fundamental frequencies. For this purpose, the full set of 62 standard internal coordinates (containing 14 redundancies) for DMNB was defined as given in Table 2. From these, a non-redundant set of local symmetry coordinates were constructed by suitable linear combinations of internal coordinates the following recommendations of Fogarasi *et al.*[24] is summarized in Table 3. The theoretically calculated force fields were transformed to this set of vibrational coordinates and used in all subsequent calculations. The experimental and theoretical FTIR and FT-Raman spectra of title molecule are shown in Figs 2 and 3, respectively. The title molecule belongs to C1 point group symmetry and all the vibrations are found to be IR and Raman active suggesting that the molecule possesses a non-centro symmetric structure, which recommends the title compound for non-linear optical applications. The observed FTIR and FT-Raman bands and harmonic frequencies for various modes of vibrations calculated by B3LYP method with 6-31G(d,p) basis set along with PED have been summarized in Table 4 for DMNB.

4.2.1 C–H vibrations

Heteroaromatic structure shows the presence of C–H stretching vibrations in the region 3100–3000 cm^{-1}. This is the characteristics region for the ready identifications of C–H stretching vibrations[25,26]. In this region, the FTIR bands observed at 3250 and 3200 cm^{-1} have been designated to C–H stretching vibrations. The in-plane C–H bending vibrations appear in the range 1300–1000 cm^{-1} in the substituted benzene[27]. The C–H in-plane bending and out-of-plane bending vibrations are appeared within the characteristic region.

4.2.2 C–C vibrations

Most of the ring vibrational modes are affected by the substitutions of functional groups. The characteristic

Table 1 — Geometrical parameters of DMNB calculated using B3LYP/6-31G(d,p) method.

Bond Lengths	Values (Å)	Experimental[a]	Bond Angles	Values (°)	Experimental[a]	Dihedral angles	Values (°)	Experimental[a]
C1–C2	1.401	1.392	C2–C1–C6	118.447	124.5	C6–C1–C2–C3	0.401	180.5
C1–C6	1.397	1.383	C2–C1–C7	120.846	120.9	C6–C1–C2–H11	–179.342	124.5
C1–C7	1.510	1.519	C6–C1–C7	120.699	120.9	C7–C1–C2–C3	–178.702	
C2–C3	1.401	1.378	C1–C2–C3	122.471	117.1	C7–C1–C2–H11	1.553	
C2–H11	1.087	0.950	C1–C2–H11	118.764	126.1	C2–C1–C6–C5	–0.247	180.3
C3–C4	1.397	1.380	C3–C2–H11	118.763	126.1	C2–C1–C6–H20	179.416	
C3–C12	1.510	0.950	C2–C3–C4	118.448	120.5	C7–C1–C6–C5	178.858	
C4–C5	1.391	1.394	C2–C3–C12	120.831	121.6	C7–C1–C6–H20	–1.477	
C4–H16	1.083	0.950	C4–C3–C12	120.713	121.6	C2–C1–C7–H8	–32.947	
C5–C6	1.391	1.413	C3–C4–C5	119.003	120.6	C2–C1–C7–H9	86.560	
C5–N17	1.473	1.483	C3–C4–H16	121.682	126.5	C2–C1–C7–H10	–153.845	
C6–H20	1.083	1.543	C5–C4–H16	119.312	126.5	C6–C1–C7–H8	147.968	
C7–H8	1.093	0.980	C4–C5–C6	122.622	125.8	C6–C1–C7–H9	–92.523	
C7–H9	1.096	0.979	C4–C5–N17	118.687	117.5	C6–C1–C7–H10	27.070	
C7–H10	1.093	0.979	C6–C5–N17	118.688	118.1	C1–C2–C3–C4	–0.401	0.045
C12–H13	1.093	0.980	C1–C6–C5	119.004	126.7	C1–C2–C3–C12	178.709	
C12–H14	1.093	0.980	C1–C6–H20	121.681	126.7	H11–C2–C3–C4	179.342	
C12–H15	1.096	0.980	C5–C6–H20	119.313	126.7	H11–C2–C3–C12	–1.546	
N17–O18	1.231	1.219	C1–C7–H8	111.406	120.5	C2–C3–C4–C5	0.246	180.5
N17–O19	1.231	1.219	C1–C7–H9	110.974	120.5	C2–C3–C4–H16	–179.417	
			C1–C7–H10	111.403	120.5	C12–C3–C4–C5	–178.865	180.5
			H8–C7–H9	107.309	109.5	C12–C3–C4–H16	1.470	
			H8–C7–H10	108.174	109.5	C2–C3–C12–H13	154.435	
			H9–C7–H10	107.379	109.5	C2–C3–C12–H14	33.539	
			C3–C12–H13	111.404	121.5	C2–C3–C12–H15	–85.956	
			C3–C12–H14	111.403	121.5	C4–C3–C12–H13	–26.474	
			C3–C12–H15	110.975	121.5	C4–C3–C12–H14	–147.369	
			H13–C12–H14	108.173	109.5	C4–C3–C12–H15	93.133	
			H13–C12–H15	107.389	109.5	C3–C4–C5–C6	–0.111	
			H14–C12–H15	107.301	109.5	C3–C4–C5–N17	–179.655	
			C5–N17–O18	117.773	117.3	H16–C4–C5–C6	179.560	
			C5–N17–O19	117.774	117.3	H16–C4–C5–N17	0.016	
			O18–N17–O19	124.452	125.4	C4–C5–C6–C1	0.112	
						C4–C5–C6–H16	–179.559	
						N17–C5–C6–C1	179.656	180.0
						N17–C5–C6–H16	–0.015	180.0
						C4–C5–N17–O18	–0.260	–89.7
						C4–C5–N17–O19	179.815	89.7
						C6–C5–N17–O18	–179.822	90.3
						C6–C5–N17–O19	0.253	–90.3

[a]Ref[22, 23]

ring stretching vibrations are assigned in the region[28] 1650–1300 cm^{-1}. Therefore, the C–C stretching vibrations of DMNB are found at 1600 and 1420 cm^{-1} in FTIR spectrum and the corresponding FT-Raman vibrations are disappeared due to functional group attachment. The theoretically computed values for C–C vibrational modes by B3LYP/6-31G(d,p) method gives excellent agreement with experimental data. Small changes in wavenumber observed for these modes are due to the changes in force constant/reduced mass ratio, resulting mainly due to addition of methyl and nitro groups.

The in-plane ring deformations[28] are observed below 1000 cm^{-1}. The in-plane bending modes predicted at 755, 559, 425, 388 and 362 cm^{-1} by B3LYP method exactly correlate with FTIR bands at 730 cm^{-1} and 595 cm^{-1} in FT-Raman spectrum. The out-of-plane ring deformation modes[29] are

Table 2 — Definition of internal coordinates of DMNB.

S. No.	Symbol	Type	Definition
		Stretching	
1–6	R_i	C–C	C1–C2, C2–C3, C3–C4, C4–C5, C5–C6, C6–C1
7–8	q_i	C–C(CH_3)	C1–C7, C3–C12
9–11	D_i	C–H	C2–H11, C4–H16, C6–H20
12	r	C–N	C5–N17
13–18	Q	C–H(CH_3)	C7–H8, C7–H9, C7–H10, C12–H13, C12–H14, C12–H15
19–20	P	N–O	N17–O18, N17–O19
		Bending	
21–26	β_i	Ring	C1–C2–C3, C2–C3–C4, C3–C4–C5, C4–C5–C6, C5–C6–C1, C6–C1–C2
27–30	α_i	C–C–C(CH_3)	C2–C1–C7, C6–C1–C7, C2–C3–C12, C4–C3–C12
31–36	σ_i	C–C–H	C1–C2–H11, C3–C2–H11, C3–C4–H16, C5–C4–H16, C1–C6–H20, C5–C6–H20
37–42	α_i	C–C–H(methyl)	C1–C7–H8, C1–C7–H9, C1–C7–H10, C3–C12–H13, C3–C12–H14, C3–C12–H15
43–48	σ_i	H–C–H(methyl)	H8–C7–H9, H8–C7–H10, H9–C7–H10, H13–C12–H14, H14–C12–H15, H13–C12–H15
49–50	Υ_i	C–C–N	C4–C5–N17, C6–C5–N17
51–52	δ_i	C–N–O	C5–N17–O18, C5–N17–O19,
53	θ_i	O–N–O	O18–N17–O19
		Out-of-plane bending	
54–56	ω	H–C–C	H11–C2–C3–C1, H16–C4–C3–C5, H20–C6–C5–C1
57–58	ω	C–C–C	C7–C1–C6–C2, C12–C3–C2–C4
59	ω	N–C–C	N17–C5–C6–C4
		Torsion	
60–65	τ	Ring	C1–C2–C3–C4, C2–C3–C4–C5, C3–C4–C5–C6, C4–C5–C6–C1, C5–C6–C1–C2, C6–C1–C2–C3
66	τ	NO_2	C5–N17–O18–O19
67–68	τ	CH_3	C6–C1–C7–(H8, H9, H10), C2–C3–C12–(H13, H14, H15)

Table 3 — Definition of local symmetry coordinates of DMNB.

S. No.	Symbol	Definition
1–6	CC	R1, R2, R3, R4, R5, R6
7–8	CC(CH_3)	q7, q8
9–11	CH	D9, D10, D11
12	CN	r12
13–14	CH_3sym	(Q13+Q14+Q15)/ √3, (Q16+Q17+Q18)/ √3
15–16	CH_3asym	(2Q13–Q14–Q15)/√6, (2Q16–Q17–Q18)/√6
17–18	CH_3asym	(Q14–Q15)/√2, (Q17–Q18)/√2
19	NO_2sym	(P19+P20)/√2
20	NO_2asym	(P19–P20)/√2
21	Rtrigd	(β21–β22+β23–β24+β25–β26)/√6
22	Rsymd	(–β21–β22+2β23–β24+β25+2β26)/√6
23	Rasymd	(–β23–β24+2β25–β26)/√2
24–25	βCCC(CH_3)	(α27–α28)/√2, (α29–α30)/√2
26–28	βCH	(σ31– σ32)/√2, (σ33–σ34)/√2, (σ35–σ36)/√2
29–30	CH_3sb	(–α37–α38–α39+σ43+σ44+σ45)/√6), (–α40–α41–α42+σ46+σ47+σ48)/√6,
31–32	CH_3ipb	(–σ43–σ44–2σ45)/√6, (–σ46–σ47–2σ48)/√6
33–34	CH_3opb	(σ43–σ45)/√2, (σ46–σ48)/√2
35–36	CH_3ipr	(–α37+2α38–α39)/√6, (–α40+2α41–α42)/√6
37–38	CH_3opr	(α38–α39)/√2, (α41–α42)/√2
39	βCCN	(ϒ49–ϒ50)/√2
40	NO_2rock	(δ51–δ52)/√2
41	NO_2twist	(δ51+δ52)/√2
42	NO_2sciss	(2θ53–δ51–δ52)/√2
43–45	γCH	ω54, ω55, ω56
46–47	γCC	ω57, ω58
48	γCN	ω59
49	Rtrigd	(τ60–τ61+τ62–τ63+τ64–τ65)/√6
50	Rsymd	(τ60–τ62+τ63+τ65)/√2
51	Rasymd	(–τ60+2τ61–τ62–τ63+2τ64–τ65)/√2
52	τNO_2	τ66
53–54	τCH_3	τ67, τ68
49	Rtrigd	(τ60–τ61+τ62–τ63+τ64–τ65)/√6
50	Rsymd	(τ60–τ62+τ63+τ65)/√2
51	Rasymd	(–τ60+2τ61–τ62–τ63+2τ64–τ65)/√2
52	τNO_2	τ66
53–54	τCH_3	τ67, τ68

existing below 800 cm^{-1}. The FT-Raman peaks observed at 490, 260, 200 and 100 cm^{-1} are attributed to out-of-plane bending vibrations. In this region we see the modes are mixed vibrational modes as evident from calculated PED results and also in agreement with the reported results. All the above assignments are satisfactorily agreeing with the literatures.

4.2.3 CH_3 (Methyl) group vibration

For the assignments of CH_3 group frequencies, basically nine fundamentals can be associated to each CH_3 group namely, CH_3 sym, symmetrical stretch; CH_3 asym, asymmetrical stretch (CH_3 ips and ops, in-plane stretch and out-of-stretch (i.e., in-plane hydrogen stretching modes)); CH_3 ipb, in-plane-

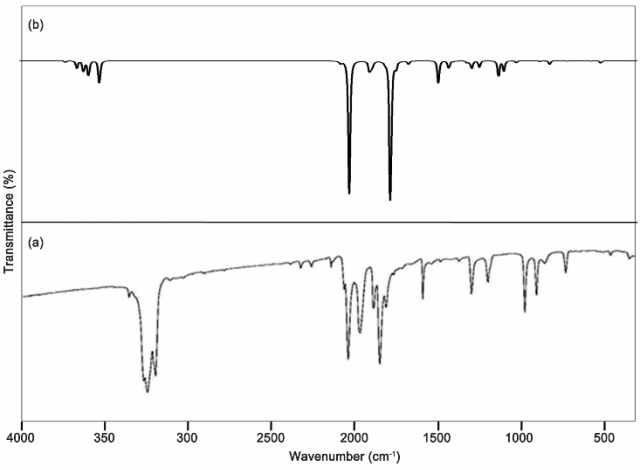

Fig. 2 — Comparison of observed and calculated FT-IR spectra of DMNB (a) observed and (b) calculated by B3LYP/6-31G(d,p).

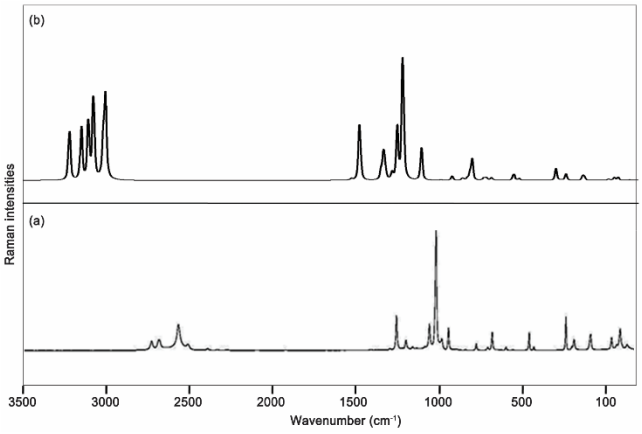

Fig. 3 — Comparison of observed and calculated FT-Raman spectra of DMNB (a) observed and (b) calculated by B3LYP/6-31G(d,p).

bending (i.e., hydrogen deformation modes); CH_3 opb, out-of-plane-bending (i.e., hydrogen deformation modes); CH_3 sb, symmetric bending; CH_3 ipr, in-plane rocking; CH3 opr, out-of-plane rocking and tCH3, twisting hydrogen bending modes. In addition to that, CH_3 ops, out-of-plane stretch and CH_3 opb, out-of-plane bending modes of CH_3 group would be expected to be depolarized for A″ symmetry species[30]. The molecule under consideration possesses two CH_3 group in the side substitution chain. The mode appears in the region 3017 and 2867 cm^{-1} are assigned to CH_3 stretching mode of vibrations[31]. But the CH_3 symmetric stretching frequency is established at 2740 cm^{-1} FT-Raman of DMNB. These assignments are also supported by literature[32] in addition to PED output. The two in-plane methyl hydrogen deformation modes are also well established[33].

Table 4 — The observed FTIR, FT-Raman and theoretically calculated frequencies by B3LYP/6-31G(d,p) method along with their assignments, IR intensities (km mol^{-1}) and Raman intensities ($Å^4$ amu^{-1}) , reduced masses (AMU) and force constants (mDyne/A)of DMNB.

S. No.	Observed wavenumbers		Calculated wavenumbers		IR Intensities	Raman intensities	Reduced masses	Force constants	[a]Vibrational assignments
	FTIR	FT-Raman	Unscaled	Scaled					
1	3250(m)		3236	3175	0.56	32.11	1.09	6.73	νCH(98)
2	3200(m)		3196	3127	2.56	71.46	1.09	6.73	νCH(97)
3			3172	3099	13.48	88.98	1.09	6.46	νCH(97)
4			3133	3065	15.18	79.82	1.10	6.38	CH_3asym(95)+βCH(61)+ βCN(41)
5			3133	3022	7.69	37.29	1.10	6.38	CH_3asym(93)+βCC(61)+νCH(40)
6			3105	3011	27.2	83.60	1.09	6.23	CH_3asym(93)+βCN(62)+ NO_2asym(53)
7			3085	2912	4.90	83.62	1.09	6.23	CH_3asym(94)+νCC(58)+CH3ipb(43)
8			3053	2845	14.67	100	1.03	5.67	CH_3sym(91)+βCH(55)+βCC(47)
9		2740(vw)	3013	2812	28.53	42.63	1.03	5.67	CH_3sym(90)+νCN(49)+βCH(38)
10			1681	1593	4.76	1.98	7.92	13.20	νCC(85)+βCH(59)+βCN(41)
11			1638	1554	0.35	57.00	5.74	9.08	νCC(82)+βCC(52)+βCH(47)
12	1600(m)		1630	1524	233.9	14.76	10.08	15.80	νCC(81)+ NO_2sym(49)+ CH_3asym(40)
13	1525(vw)		1519	1485	5.15	1.64	1.84	2.50	NO_2asym(91)+νCN(52)+νCC(42)
14			1507	1438	18.15	12.15	1.27	1.72	νCC(98)+ CH_3sym(47)+νCN(39)
15			1502	1485	11.28	14.99	1.05	1.39	νCC(82)+βCN(51)+βCC(44)
16			1492	1446	1.00	23.31	1.04	1.39	CH_3ipb(75)+βCC(52)+νCH(38)
17			1473	1429	2.38	4.83	1.50	1.97	νCC(75)+νCN(47)+ CH_3asym(36)
18			1457	1417	0.04	7.91	2.20	2.76	CH_3ipb(71)+ NO_2sym(62)+βCH(41)
19	1420(vw)		1429	1376	2.73	38.13	1.26	1.52	νCC(72)+ CH_3ipb(57)+βCN(39)
20			1406	1327	0.26	21.08	1.22	1.47	NO_2sym(81)+βCH(52)+βCC(32)
21			1397	1308	302.0	59.75	13.89	15.98	CH_3opb(71)+CH3asym(47)+νCN(35)
22	1340(s)	1320(m)	1366	1286	12.05	0.33	6.06	6.67	CH_3opb(69)+βCN(52)+γCH(41)
23			1300	1249	0.01	1.26	1.30	1.30	βCH(61)+ NO_2sym(41)+βCC(29)
24	1260(m)	1250(vw)	1296	1223	6.15	34.37	4.91	4.86	CH_3sb(59)+νCN(51)+βCH(43)
25			1187	1157	0.20	0.68	1.37	1.14	βCH(55)+νCN(35)+ βCC(27)
26			1126	1108	40.15	4.46	1.46	1.09	βCH(52)+ CH_3sym(41)+νCH(29)
27		1080(w)	1068	1025	11.03	1.36	1.55	1.04	CH_3sb(62)+ CH_3ipb(47)+βCH(29)
28		1050(vs)	1047	1021	4.80	1.30	1.51	1.01	CH_3ipr(56)+ NO_2sym(48)+νCN(32)
29			1031	1008	1.27	1.96	1.48	0.95	NO_2sciss(49)+βCC(42)+βCH(22)

(*Contd.*)

Table 4 — The observed FTIR, FT-Raman and theoretically calculated frequencies by B3LYP/6-31G(d,p) method along with their assignments, IR intensities (km mol^{-1}) and Raman intensities ($Å^4$ amu^{-1}) , reduced masses (AMU) and force constants (mDyne/A)of DMNB.

S. No.	Observed wavenumbers		Calculated wavenumbers		IR Intensities	Raman intensities	Reduced masses	Force constants	[a]Vibrational assignments
	FT-IR	FT-Raman	Unscaled	Scaled					
30	1015(vs)		1016	996	0.30	7.35	1.73	1.07	CH_3opr(59)+βCN(31)+βCC(25)
31		1000(vw)	1004	955	0.21	20.51	4.59	2.79	νCC(45)+βCN(32)+βCH(23)
32	980(s)	985(w)	966	945	3.33	0.17	3.59	1.97	NO_2wagg(51)+CH_3sb(42)+βCN(32)
33			949	931	3.40	2.80	1.39	0.74	νCN(68)+βCH(42)+νCC(27)
34	920(w)		936	912	13.98	2.51	4.80	2.48	CH_3ipr(62)+Rasymd(41)+βCH(23)
35			908	869	0.23	2.72	1.30	0.63	NO_2twist(58)+γCH(47)+βCN(27)
36			894	854	12.22	0.14	1.40	0.66	CH_3opr(56)+ NO_2wagg(51)+βCH(23)
37		800(vw)	786	765	33.01	7.18	10.30	3.75	γCH(65)+βCC(42)+βCN(22)
38	730(w)		755	723	17.85	1.66	5.44	1.83	Rasymd(61)+γCH(49)+CH_3sb(21)
39		690(m)	685	669	3.47	0.06	2.68	0.74	γCH(57)+ CH_3ipb(42)+γCN(32)
40		595(vw)	575	559	0.19	0.00	5.10	0.99	βCC(53)+βCH(42)+νCN(23)
41			552	521	1.48	10.42	4.60	0.82	γCH(43)+βCC(32)+βCH(12)
42	525(vw)		526	512	0.25	0.37	3.16	0.51	NO_2rock(51)+βCH(42)+ CH_3opr(19)
43		490(m)	497	481	1.77	5.64	4.29	0.62	γCC(49)+γCH(39)+γCN(18)
44			446	425	4.81	0.17	4.61	0.67	Rsymd(61)+ NO_2twist(48)+γCH(17)
45			405	388	0.01	2.98	4.17	0.40	βCC(59)+βCH(37)+βCN(17)
46			397	362	0.93	3.19	7.93	0.73	Rtrigd(51)+ NO_2rock(21)+γCC(16)
47		260(s)	262	241	0.84	1.26	2.64	0.10	γCC(39)+γCN(23)+γCH(12)
48			231	212	0.01	2.44	3.15	0.09	tRasymd(52)+Rsymd(31)+γCN(18)
49			210	189	3.38	2.50	3.32	0.08	βCN(44)+βCC(29)+βCH(16)
50		200(vw)	200	158	1.22	0.00	5.22	0.12	tRsymd(43)+βCH(12)+γCN(23)
51		100(w)	145	125	0.15	0.41	4.57	0.05	tRtrigd(45)+ CH_3opb(22)+γCH(12)
52			91	78	0.00	0.36	10.58	0.01	γCN(36)+γCH(17)+γCC(11)
53			59	41	0.55	0.93	1.01	0.00	t CH_3 (25)+γCN(18)+γCH(12)
54			35	29	0.24	0.28	1.01	0.00	t CH_3 (22)+γCC(15)+Rsymd(11)

[a]Only contributions larger than 10% are given. Experimental relative intensities are abbreviated as follows: vs-very strong, s-strong, m-medium, w-weak, vw-very weak. Abbreviations; ν-stretching, sym-symmetric stretching, asym-asymmetric stretching, β-in-plane bending, γ-out-of-plane bending, ipb-in-plane bending, opb-out-of-plane bending, sb-symmetric bending, ipr-in-plane rocking, opr-out-of-plane rocking, d-deformation, R-ring,trig-trigonal, sciss-scissoring, rock-rocking, wagg-wagging, twist-twisting, t-torsion.

We have observed the symmetrical methylde formation mode CH_3 sb at 1260 cm^{-1} in the FTIR spectrum, 1250 and 1080 cm^{-1} in FT-Raman spectrum for DMNB. The out-of-plane bending methyl deformation mode CH_3opb appeared at 1340 cm^{-1} in FTIR spectrum and1320 cm^{-1} in FT-Raman spectrum. The bands obtained at 1015, 920 and 1050 cm^{-1} in FTIR and FT-Raman spectra are assigned to CH_3 in-plane and out-of-plane rocking modes. The assignment of the bands at 41 and 29 cm^{-1} calculated by B3LYP method is attributed to methyl twisting mode.

4.2.5 NO_2 Vibrations

Aromatic nitro compounds have strong absorptions due to the asymmetric and symmetric stretching vibrations of the NO_2 group at 1570−1500 cm^{-1} and 1370−1300 cm^{-1}, respectively[34,35]. Hydrogen bonding has a little effect on the NO_2 asymmetric stretching vibrations[27]. In title molecule, the very weak FT-Raman band at 1525 cm^{-1} has been assigned to asymmetric vibration. The PED of these modes contributes 91% for asymmetric stretching. The other vibrations of NO_2 group (scissoring, rocking, wagging and twisting) contribute to several normal modes in the lower frequency region. Aromatic nitro compounds have a band of weak to medium intensity in the region[36] 590−500 cm^{-1} due to the out-of-plane bending (wagging and twisting) of the NO_2 group. The wagging vibration is observed at 980, 985cm^{-1} in FTIR and FT-Raman spectra (calculated 945 cm^{-1}). Likewise, the in-plane (scissoring and rocking) NO_2 deformation vibrations have a week to medium absorption in the region[37,38] 775−660 cm^{-1}. In the present case, rocking vibration is observed in FTIR spectrum at 525 cm^{-1}. Also the calculated rocking vibration is 512 cm^{-1} by B3LYP method. Hence it is

clear that, this assignment is in line with the literature and the vibrational frequency is not affected.

5 Natural Bond Orbital (NBO) Analysis

For studying hybridization, conjugative interactions, covalence effects and charge transfer in polyatomic wave functions, NBO analysis is one of the efficient methods. The information from the first-order density matrix of the DFT calculation was extracted to develop a unique set of atomic hybrids and bond orbitals which leads to "Lewis structure". It helps in easy understanding of the bonding in molecules. Delocalization of electron density between occupied Lewis-type (bond or lone pair) NBO orbitals and formally unoccupied (antibond or Rydberg) non-Lewis NBO orbitals correspond to a stabilizing donor-acceptor interaction which helps in the investigation of inter-molecular/intra-molecular interactions among bonds. In the present work utilizing the second-order micro-disturbance theory analysis we have reported some of the electron donor orbital, acceptor orbital and the interacting stabilization energy. The intensity of the interaction between electron donors and electron acceptors, i.e., the more donating tendency from electron donors to electron acceptors depends on the $E^{(2)}$ value. The hyper conjugative interaction energy was deduced from the second-order perturbation approach[39]:

$$E^{(2)} = -n_{\sigma}\frac{\langle\sigma|F|\sigma\rangle^2}{\varepsilon_{\sigma^*}-\varepsilon_{\sigma}} = -n_{\sigma}\frac{F_{ij}^2}{\Delta E} \quad \ldots (2)$$

where $\langle\sigma|F|\sigma\rangle^2$, or F_{ij}^2 is the Fock matrix element between the *i* and *j* NBO orbital, ε_{σ^*} and ε_{σ} are the energies of σ and σ* NBO's, and n_{σ} is the population of the donor σ orbital.

The larger the $E^{(2)}$ value the more intensive is interaction, the greater the extent of conjugation of the whole system[39]. Hyperconjugation may be given as a stabilizing effect that arises from overlap between an occupied orbital with another neighboring electron deficient orbital when these orbitals are properly oriented. The most important interaction between "filled" (donor) Lewis type NBOs and "empty" (acceptor) non-Lewis NBOs is reported in Table 5. The co-planarity of nitro group with the ring increases conjugation between them which further supports the electron delocalization from the ring to the nitro group. The calculated natural orbital occupancy (number of electron (or) "natural population" of the orbital), it is noted that the maximum occupancies 1.994 and 1.993 are obtained for BD(N17–O18) and BD(N17–O19), respectively, and also corresponding *sp* composition are also tabulated. Therefore, the results suggest that the

Table 5 – Selected NBO results showing formation of Lewis and non-Lewis orbitals for DMNB using B3LYP/6-31G level of theory.

Bond (A–B)	ED/Energy (a.u.)	ED_A (%)	ED_B (%)	NBO	S%	P%
BD(C1–C7)	1.982	51.34	48.66	0.7765($SP^{2.27}$)C+0.6976 ($SP^{2.87}$)C	30.55	69.43
					25.85	74.11
BD(C3–C12)	1.982	51.34	48.66	0.7165($SP^{2.27}$)C + 0.6976($SP^{2.27}$)C	30.55	69.42
					25.85	74.11
BD(C5–N17)	1.990	3748	62.52	0.6122($SP^{3.08}$)C+ 0.7907($SP^{1.48}$)N	24.49	75.38
					40.39	59.59
BD(C7–H8)	1.988	62.07	37.93	0.7878($SP^{3.04}$)C+0.6159($SP^{0.00}$)H	24.76	75.19
					99.96	0.04
BD(C7–H9)	1.979	62.39	37.61	0.7898($SP^{3.08}$)C+0.6133($SP^{0.00}$)H	24.52	75.43
					99.95	0.05
BD(C7–H10)	1.988	62.25	37.75	0.7890($SP^{3.03}$)C+0.6144($SP^{0.00}$)H	24.82	75.14
					99.96	0.04
BD(C12–H13)	1.988	62.24	37.76	0.7889($SP^{3.03}$)C+0.6145($SP^{0.00}$)H	24.82	75.13
					99.96	0.04
BD(C12–H14)	1.988	62.08	37.92	0.7879($SP^{3.04}$)C+0.6158($SP^{0.00}$)H	24.52	75.20
					99.96	0.04
BD(C12–H15)	1.979	62.38	37.62	0.7898($SP^{3.08}$)C+0.6133($SP^{0.00}$)H	24.52	75.43
					99.95	0.05
BD(N17–O18)	1.994	51.18	48.82	0.7154($SP^{2.36}$)N+0.6984($SP^{5.02}$)O	29.70	70.19
					16.58	83.26
BD(N17–O18)	1.982	39.87	60.13	0.6314($SP^{1.00}$)N+0.7755($SP^{1.00}$)O	0.05	99.84
					0.23	99.84
BD(N17–O19)	1.993	51.18	48.82	0.7154($SP^{2.36}$)N+0.6987($SP^{5.02}$)O	29.70	70.19
					16.58	83.26

N17–O18, and N17–O19 bond lengths of these compounds are essentially controlled by the *p* character of these hybrid orbitals and also by the nature of the N17–O18, and N17–O19 bonds.

5.1 Second order perturbation theory analysis

Delocalization of the electron density between occupancies Lewis type (bond (or) lone pair) NBO orbital and formally unoccupied (anti-bond (or) Rydberg) non-Lewis NBO orbital corresponding to a stabilizing donor–acceptor interaction have been performed at B3LYP/6-31G(d,p) level of theory. The energy of these interactions can be estimated by the second order perturbation theory[40,41]. Table 6 lists the calculated second-order interaction energies ($E^{(2)}$) between the donor-acceptor orbital in DMNB.

Table 6 – Second order perturbation theory analysis of Fock matrix on NBO basis for DMNB using B3LYP method with 6-31G(d,p) basis set.

Donar NBO(*i*)	Acceptor NBO (*j*)	[a]$E^{(2)}$ (kcal/mol)	[b]$E(i)$-$E(j)$ (a.u)	[c]$F(i,j)$ (a.u.)
BD(C1–C2)	BD*(C1–C7)	1.30	1.09	0.034
BD(C1–C2)	BD*(C3–C12)	3.28	1.09	0.053
BD(C1–C2)	BD*(C7–H9)	2.12	0.74	0.039
BD(C1–C2)	BD*(C7–H10)	0.70	0.74	0.023
BD(C1–C6)	BD*(C1–C7)	1.18	1.09	0.032
BD(C1–C6)	BD*(C5–N17)	4.65	1.01	0.062
BD(C1–C7)	BD*(C7–H9)	0.58	1.09	0.022
BD(C1–C7)	BD*(C7–H10)	0.51	1.09	0.021
BD(C3–C4)	BD*(C3–C12)	1.18	1.09	0.032
BD(C3–C4)	BD*(C5–N17)	4.67	1.01	0.062
BD(C3–C4)	BD*(C12–H14)	0.80	0.74	0.024
BD(C3–C4)	BD*(C12-H14)	2.18	0.74	0.040
BD(C3–C12)	BD*(C1–C2)	2.60	1.18	0.049
BD(C3–C12)	BD*(C2–C3)	1.56	1.18	0.038
BD(C3–C12)	BD*(C3–C4)	1.66	1.18	0.040
BD(C3–C12)	BD*(C4–C5)	2.78	1.16	0.051
BD(C3–C12)	BD*(C12–H13)	0.51	1.09	0.021
BD(C3–C12)	BD*(C12–H15)	0.58	1.09	0.022
BD(C4–C5)	BD*(C3–C12)	3.05	1.10	0.052
BD(C4–C5)	BD*(N17–O19)	2.33	0.96	0.043
BD(C4–H16)	BD*(C5–N17)	0.65	0.82	0.021
BD(C5–C6)	BD*(C1–C7)	3.06	1.10	0.052
BD(C5–C6)	BD*(N17–O18)	35.38	0.12	0.062
BD(C5–N17)	BD*(C1–C6)	1.35	1.40	0.039
BD(C5–N17)	BD*(C3–C4)	1.35	1.40	0.039
BD(C5–N17)	BD*(C4–C5)	0.72	1.38	0.028
BD(C6–H20)	BD*(C5–N17)	0.65	0.82	0.021
BD(C7–H8)	BD*(C1–C6)	3.04	1.09	0.052
BD(C7–H9)	BD*(C1–C2)	3.54	0.54	0.043
BD(C7–H10)	BD*(C1–C2)	3.00	1.09	0.051
BD(C12–H13)	BD*(C2–C3)	3.04	1.09	0.052
BD(C12–H13)	BD*(C3–C4)	0.68	0.54	0.019
BD(C12–H14)	BD*(C3–C4)	2.99	1.09	0.051
BD(C12–H15)	BD*(C3–C4)	0.51	1.09	0.021
BD(N17–O18)	BD*(N17–O19)	0.61	1.12	0.024
BD(N17–O18)	BD*(C5–C6)	5.17	0.41	0.045
BD(N17–O18)	BD*(N17–O18)	6.83	0.24	0.044
BD(N17–O19)	BD*(C4–C5)	1.27	1.44	0.038

[a]$E^{(2)}$ means energy of hyper conjugative interactions (stabilization energy). [b]Energy difference between donor and acceptor *i* and *j* NBO orbitals. [c]$F(i,j)$ is the Fock matrix element between *i* and *j* NBO orbital.

The stabilization energy $E^{(2)}$ associated with the hyper conjugative interactions viz. BD(C5–C6)→BD *(N17–O18) is obtained 35.38 kcal/mol. It is worth mentioning that the differences in stabilization energies reported in Table 7 are reasonable.

6 Non-linear Optical (NLO) Properties

Based on the finite-field approach, the non-linear optical (NLO) parameters such as dipole moment, mean polarizability, anisotropy polarizability and first order hyperpolarizability of DMNB molecule are calculated using B3LYP level with 6-31G(d,p) basis set for more reliability. The numerical values of above mentioned parameters are listed in Table 7. In the presence of an external electric field (E), the energy of the system is a function of the electric field. First hyperpolarizability is a third-rank tensor that can be described by a 3×3×3 matrix. The 27 components of the 3D matrix can be reduced to 10 components because of the Kleinman symmetry[42]. The components of β are defined as the coefficients in the Taylor series expansion of energy in an external electric field.

When an external electric field is weak and homogeneous, Taylor series expansion becomes:

$$E = E^0 - \frac{\mu_i F_i}{1!} - \frac{\alpha_{ij} F_i F_j}{2!} - \frac{\beta_{ijk} F_i F_j F_k}{3!} - \frac{\gamma_{ijki} F_i F_j F_k F_l}{4!} + \cdots \quad \ldots (3)$$

where E is the energy of the unperturbed molecules, F_i is the field at origin and μ_i, α_{ij}, β_{ijk} and γ_{ijkl} are the components of dipole moment, polarizability, first hyperpolarizability and the second hyperpolarizability, respectively.

In this study, mean polarizability, anisotropy of polarizabiliy and molecular first hyperpolarizability of title compound are investigated. The polarizability and hyperpolarizability tensors (α_{xx}, α_{xy}, α_{yy}, α_{xz}, α_{yz}, α_{zz} and β_{xxx}, β_{xxy}, β_{xyy}, β_{yyy}, β_{xxz}, β_{xyz}, β_{yyz}, β_{xzz}, β_{yzz}, β_{zzz}) can be obtained by a frequency job output file of Gaussian software. However, α and β values of Gaussian output are in atomic units (a.u.) so they have been converted into electronic units (esu) (α; 1 a.u. = 0.1482×10^{-24} esu, β; 1 a.u. = 8.6393×10^{-33} esu). The total static dipole moment μ, mean polarizability (α_{tot}), anisotropy of polarizability (Δα) and the average value of the first hyperpolarizability $\langle\beta\rangle$ can be calculated using the following equations:

$$\mu = \left(\mu_x^2 + \mu_y^2 + \mu_z^2\right)^{1/2} \quad \ldots (4)$$

$$\alpha_{tot} = \frac{1}{3}\left(\alpha_{xx} + \alpha_{yy} + \alpha_{zz}\right) \quad \ldots (5)$$

$$\Delta\alpha = \frac{1}{\sqrt{2}}\left[\left(\alpha_{xx} - \alpha_{yy}\right)^2 + \left(\alpha_{yy} - \alpha_{zz}\right)^2 + \left(\alpha_{zz} - \alpha_{xx}\right)^2 + 6\alpha_{xz}^2 + 6\alpha_{xy}^2 + 6\alpha_{yz}^2\right]^{\frac{1}{2}} \quad \ldots (6)$$

$$\langle\beta\rangle = \left[\left(\beta_{xxx} + \beta_{xyy} + \beta_{xzz}\right)^2 + \left(\beta_{yyy} + \beta_{yzz} + \beta_{yxx}\right)^2 + \left(\beta_{zzz} + \beta_{zxx} + \beta_{zyy}\right)^2\right]^{\frac{1}{2}} \quad \ldots (7)$$

The calculated values of dipole moment (μ) were found to be 3.8602 Debye. The highest value of dipole moment is observed for component μ_x, μ_y and μ_z. In this direction, this value is equal to 5.0860, 0.0013 and 0.0815 Debye. The calculated polarizability α_{ij} have non-zero and zero values are dominated by the diagonal components. Meanpolarizability (α_{tot}) calculated as -23.4512×10^{-24} and anisotropy of polarizability (Δα) is equal to 0.2378×10^{-24} esu for title molecule. The first hyperpolarizability values β of the title compound are equal to 0.8974×10^{-33} esu. The magnitude of the molecular hyperpolarizability β, is one of important key factors in a NLO system.

Table 7 — Dipole moment μ (Debye (D)), mean polarizability α_{tot} ($\times10^{-24}$esu), anisotropypolarizability Δα ($\times10^{-24}$esu) and first hyperpolarizability $\langle\beta\rangle$ ($\times10^{-31}$esu) for DMNB obtained by B3LYP level with the 6-31G(d,p) basis set.

Parameters	B3LYP/6-31G	Parameters	B3LYP/6-31G
μ_x	5.0860	β_{xxx}	35.181
μ_y	0.0013	β_{xxy}	–0.0137
μ_z	0.0815	β_{xyy}	–7.155
μ	3.8602	β_{yyy}	0.0137
α_{xx}	–71.42	β_{xxz}	–0.4820
α_{yy}	–58.51	β_{xyz}	–0.0016
α_{zz}	–64.03	β_{yyz}	0.1688
α_{xy}	0.0019	β_{xzz}	10.855
α_{yz}	0.0009	β_{yzz}	0.0096
α_{xz}	–0.1738	β_{zzz}	1.3522
α_{tot}	–23.4512	$\langle\beta\rangle$	0.8974
Δα	0.2378		

7 UV-Analysis

The UV-Vis absorption spectrum of the DMNB is recorded in the range 100-800 nm. All the structures allow strong π-π* and σ-σ* transition in the UV-Vis region with high extinction coefficients. The calculated results involving the excitation energies (eV), oscillator strength (f) and wavelength (nm) using TD-B3LYP/6-31G(d,p) level of theory and measured experimental wavelength in nm is given in Table 8. It is evident from the table, that the calculated absorption maxima values have been found to be 675.17, 585.39 and 239.97 nm with corresponding experimental value is 400 nm.

The experimental UV-Vis absorption spectrum is shown in Fig. 4.

8 NMR Spectral Analysis

The ^{13}C and ^{1}H NMR chemical shifts are calculated within *gauge independent atomic orbital* (*GIAO)* method using B3LYP /6-31G(d,p) method. A comparison of the experimental and theoretical spectra can be very useful in making correct assignments and understanding the basic chemical shift molecular structure relationship. The experimental ^{13}C and ^{1}H NMR spectra of the title compound are given in Fig. 5 ((a) ^{13}C and (b) ^{1}H)). In Table 9, the experimental and the theoretical ^{13}C and ^{1}H isotropic chemical shifts in ppm for the title compound are given. The ^{13}C chemical shift values for all calculations have the range from 158.618 to 33.456 ppm at B3LYP/6-31G(d,p) level of theory in average for DMNB. Downfield and upfield chemical shift values observed at 158 and 33 ppm of carbons C1 and C7 are due to electron donating effect of methyl group. The carbon atoms C2, C3, C4, C5 and C6 are significantly observed in the upfield with chemical shift values 78, 143, 123, 138 and 79 ppm, respectively, which reveals that the influences of the electronegative nitrogen and methyl group atoms are negligibly small and their signal are observed in the normal range.

The ^{1}H chemical shift values for all calculations have 8.4587 from 3.6214 ppm at B3LYP/6-31G(d,p) method in the average for DMNB molecule. As can be seen from Table 9, theoretical ^{13}C and ^{1}H chemical shift results of the title compound are generally closer to the corresponding experimental chemical shift

Table 8 — Experimental and theoretical absorption frequencies of DMNB calculated using TD-B3LYP/6-31G(d,p) level of theory.

Energy states	Oscillator strength	Calculated band gap (eV/nm)	Experimental band gap (nm)
Excited State 1	Singlet-A (f = 0.0027)	1.0034eV/239.97 nm	
47 –> 51	–0.48108		
49 –> 51	0.51347		
Excited State 2	Singlet-A (f = 0.0151)	1.8504eV/675.17 nm	
44 –> 51	–0.26911		
47 –> 51	0.46457		
48 –> 51	–0.11099		
49 –> 51	0.43996		
Excited State 3	Singlet-A (f = 0.0043)	2.1259eV/585.39 nm	400
43 –> 51	–0.11256		
44 –> 51	0.35717		
45 –> 51	–0.14243		
46 –> 51	0.15488		
47 –> 51	0.53557		
48 –> 51	0.16979		
49 –> 51	0.16985		

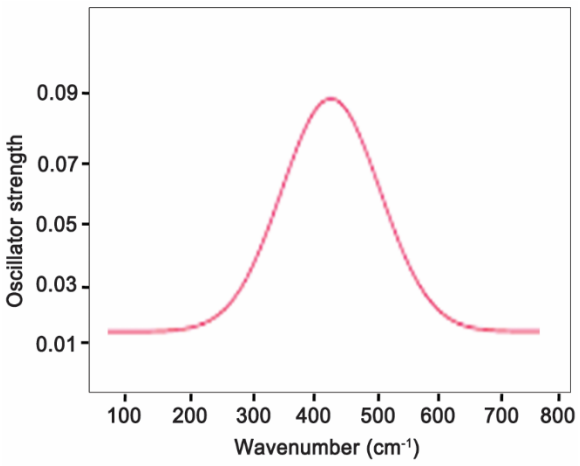

Fig. 4 — The UV-Visible spectrum of DMNB.

Table 9 — Experimental and theoretical ^{13}C and ^{1}H chemical shift (ppm) of DMNB.

Atoms	Isotropic chemical shielding tensor (σ in ppm)	Theoretical shift (ppm)	Experimental shift (ppm)
C1	24.7167	158.618	154
C2	45.1169	78.639	78
C3	52.3541	143.395	143
C4	52.2087	130.649	123
C5	45.1136	137.919	138
C6	23.5617	85.289	79
C7	45.6321	33.456	22
C12	52.6974	71.432	-
H8	24.5982	7.3333	7.4
H9	23.5073	8.4587	7.8
H10	18.4569	5.4876	-
H11	24.3874	3.6214	2.7
H13	21.6587	5.5473	-
H14	17.2154	4.6541	-
H15	15.8964	3.8925	-
H16	21.3541	5.1479	-
H20	25.7496	4.4215	-

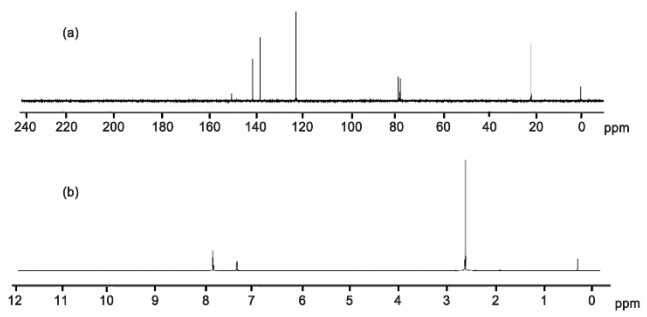

Fig. 5 — The experimental (a) ^{13}C and (b) ^{1}H NMR spectra of DMNB.

data except for C12 atom. The small shifts can be explained as a consequence of the change in the molecular environment.

9 Conclusions

The FTIR, FT-Raman, UV-Vis and ^{13}C and ^{1}H NMR spectra of the compound DMNB have been recorded and analyzed. The detailed interpretations of the vibrational spectra have been carried out. The observed wavenumbers are found to be in good agreement with the calculated values. The optimized geometrical parameters were calculated and compared with the literature XRD data. NLO investigations on the compound which have benzene ring and substituted by various electron donating or withdrawing atom or group have been fulfilled. The title compounds exhibited good NLO property much greater than that of urea. The NBO analysis predicts the interaction between lone pair and acceptor bonds with in the molecule. The donor-acceptor interaction, as obtained from NBO analysis could fairly explains the decreases of occupancies of σ bonding orbital and the increases of occupancy of π* antibonding orbital's. The compound exhibits strong effective intra-molecular charge transfer and shows the second order non-linearity. The good correlation between the UV-Vis, absorption maxima and calculated electronic absorption maxima are found. The obtained optimized geometric parameters, ^{13}C and ^{1}H NMR chemical shifts results seemed to be in a good agreement with experimental data.

References

1 Sundaraganesan N, Anand B, Meganathan C & Dominic J B, *Spectrochim Acta A*,68 (2007) 561.
2 Halliwell B & Gutteridge J M C, *Free radicals in biology and medicine*, 2nd Edn, (Oxford University Press: Oxford), 1989.
3 Gugumus F, *Oxidation inhibition in organic materials*, (CRC Press: Boca Raton), 1990.
4 Suryanarayana V, Pavan K A, Ramana R G & Pandey G C, *Spectrochim Acta A*, 48 (1992) 1481.
5 Krishnakumar V, Jayamani N, Mathammal R, *J Raman Spectros*, 40 (2009) 936.
6 Muralidhar R P & Ramana R G, *J Raman Spectros*, 20 (1989) 529.
7 Clarkson J & Ewen S W, *J Mol Struct*, 655 (2003) 413.
8 Singh D K, Srivastava S K & Asthana B P, *Vib Spectros*, 56 (2011) 26.
9 Frisch M J, Nielsen A B & Holder A J, *Gaussview user's manual, Gaussian Inc*, Pittsburgh, PA, 2009.
10 Becke A D, *J Chem Phys*, 98 (1993) 5648.
11 Lee C, Yang W & Parr R G, *Phys Rev B*, 37 (1988) 785.
12 Pulay P, Fogarasi G, Pongor G, Boggs J E & Vargha A, *J Am Chem Soc*,105 (1983) 7037.
13 Fogarasi G, Pulay P & Durig J R (Ed) *Vibrational spectra and structure*, (Elsevier: Amsterdam), 14 (1985) 125.
14 Sundius T, *Vib Spectrosc*, 29 (2002) 89.
15 MOLVIB (V.7.0): *Calculation of harmonic force fields and vibrational modes of molecules*, QCPE Program No. 807, 2002.
16 Young D C, *Computational chemistry: A practical guide for applying techniques to real world problems (Electronic)*, (John Wiley and Sons Inc: New York), 2001.
17 Sundaraganesan N, IIlakiamani S, Saleem H, Wojciechowski P M & Michalska D, *Spectrochim Acta A*, 61 (2005) 2995.
18 Keresztury G, Chalmers J M, Griffiths P R (Eds), *Raman spectroscopy: Theory in hand book of vibrational spectroscopy*, (John Wiley & Sons Ltd: New York), 2002.
19 Keresztury G, Holly S, Besenyei G, Varga J, Wang A Y & Durig J R, *Spectrochim Acta A*, 49 (1993) 2007.
20 Karabacak M, Karagoz D & Kurt M, *Spectrochimica Acta A*, 61 (2009) 2995.
21 Sundaraganesan N, Kalaichelvan S, Meganathan C, Dominic J B & Cornard J, *Spectrochimica Acta A,*71 (2008) 898.
22 Patil S & Bugarin A, *Acta Cryst*, 70 (2014) 224.
23 Skakle J M S, Gojdka B & Wardell J L, *Acta Cryst*, 62 (2006)1001.
24 Saravanan S P, Sankar A & Parimala K, *J Mol Struct*, 1127 (2017) 784.
25 Arivazhagan M & Krishnakumar V, *Indian J Pure Appl Phys*, 40 (2002) 72.
26 Parimala K & Balachandran V, *Spectrochim Acta A*, 110 (2013) 269.
27 Sundaraganesan N, Meganathan C, Dominic J B, Mani P & Jayaprakash A, *Spectrochim Acta A*, 71 (2008) 1134.
28 Dollish F R, Fateley W G & Bentley F F, *Characteristic Raman frequencies of organic compounds*, (Wiley: New York), 1974.
29 Karabacak M, Cinar Z & Cinar M, *Spectrochim Acta A*,85 (2012) 241.
30 Varsanyi G, *Assignments for vibrational spectra of seven hundred benzene derivatives*, Vols. 1–2, (Academic Kiaclo: Budapet), 1973.
31 Gunasekaran S, Seshadri S, Muthu S, Kumaresan S & Arunbalaji R, *Spectrochim Acta A*, 70 (2008) 550.
32 Parimala K & Balachandran V, *Spectrochim Acta A*, 81 (2011) 711.
33 Krishnakumar V, Keresztury G, Sundius T & Seshadri S, *Spectrochim Acta A*, 68 (2007) 845.
34 Silverstein M, Clayton B G & Morrill C, *spectrometric identification of organic compounds*, (Wiley: New York), 1981.
35 Lin-Vien D, Colthup N B, Fateley W G & Grasselli J G, *The handbook of infraredand raman characteristic frequencies of organic molecules*, (Academic Press: Boston, M A), 1991.
36 George S, *Infrared, raman characteristics group frequencies, tables and charts*, 3rd Edn, (Wiley: Chichester), 2001.
37 Balachandran V & Parimala K, *J Mol Struct*, 1007 (2012) 136.
38 Kanna R R A& Syam S N, *SpectrochimActaA*, 49 (1993) 1691.
39 Dennington R I, Keith T, Millam J, Eppinnett J K & Hovell W, *Gauss View Version* 3.0, 2003.
40 Endredi H, Billes F & Keresztury G, *J Mol Struct (Theochem)*, 677 (2004) 211.
41 Hubert Joe I, Kostova I, Ravikumar C, Amalanathan M & Pinzaru S C, *J Raman Spectrosc*, 40 (2009) 1033.
42 Kleinman D A, *Phys Rev*, 126 (1962) 1977.